Applied Catalysis B: Environmental 162 (2015) 210–216

Contents lists available at ScienceDirect

Applied Catalysis B: Environmental

journal homepage: www.elsevier.com/locate/apcatb

How CdS nanoparticles can influence TiO_2 nanotube arrays in solar energy applications?

M. Qorbani [a], N. Naseri [a], O. Moradlou [b], R. Azimirad [c], A.Z. Moshfegh [a,d,*]

[a] Department of Physics, Sharif University of Technology, P.O. Box 11155-9161, Tehran, Iran
[b] Department of Chemistry, Faculty of Sciences, Alzahra University, P.O. Box: 19938-93973, Tehran, Iran
[c] Malek-Ashtar University of Technology, Tehran, Iran
[d] Institute for Nanoscience and Nanotechnology, Sharif University of Technology, P.O. Box 14588-89694, Tehran, Iran

ARTICLE INFO

Article history:
Received 8 January 2014
Received in revised form 2 June 2014
Accepted 27 June 2014
Available online 5 July 2014

Keywords:
TNA
Cadmium sulfide
Redox reactions
Visible light

ABSTRACT

In this study, titanium dioxide (TiO_2) nanotube array (TNA) films are fabricated via anodization of titanium (Ti) sheet. After annealing, the films consisted of well ordered, vertically oriented TNAs of 125 ± 6 nm diameter, 38 ± 3 nm wall thickness, and 2.9 ± 0.3 μm in length. Cadmium sulfide (CdS) nanoparticles are deposited on the synthesized TNAs by sequential-chemical bath deposition (S-CBD) method with different immersion cycle (n) to produce heterogeneous TNA/CdS-n (n = 10, 20 and 30) nanostructures. UV–visible absorption spectra of the samples revealed that the absorption edge of CdS modified TNAs was shifted to a higher wavelength with respect to the pure TNAs indicating band gap reduction of the TNA/CdS-n. Photocurrent response of the samples was changed with n, and the maximum photocurrent density (at steady state) of 28 ± 1 mA/cm^2 (or 70 ± 2 mA/W) was obtained for the TNA/CdS-20 photoanode which is about 30 times higher than one for the pure TNA under similar condition.

1. Introduction

Increasing human population and industrialization, global warming and ozone layer depletion a result of fossil fuels consumption are among major challenges for scientists, technologists and policy makers. Moreover, the rapid growth of many developing economies, the need for both clean and renewable sources of energy is unavoidable. One of the most interesting options is the wide-scale utilization of hydrogen (H_2) as a clean fuel and recyclable energy carrier [1]. Unfortunately, up to now, commercial H_2 production is mostly based on use of fossil fuels, leading to large CO_2 releases resulted in global warming. To reduce this problem, H_2 gas generated from water in solar radiation as a renewable energy sources such as H_2 production under photocatalytic water splitting over nanostructures has attracted many attentions in recent years [2,3].

The most well-known scientific contribution that triggered the development of this method was pioneered by Fujishima and Honda [4], describing photocatalytic water splitting in a photoelectrochemical (PEC) cell using a TiO_2 electrode. Up to now, many researchers have investigated water photoelectrolysis using various forms of semiconductors such as particulate [5,6] or thin films [7] photoanodes, which is interesting and also a challenging topic currently. But there are limited studies on detailed understanding of PEC measurements.

One of the semiconductors which have been extensively used in solar and PEC cells is Titanium dioxide [8–10]. Photoelectrochemical properties of nanostructured TiO_2 photoanodes have been studied intensively due to its excellent photochemical stability, well-known wide band gap semiconducting nature and high surface area of interface with electrolyte [11,12]. Since the first report on fabrication of highly ordered TiO_2 nanotube arrays (TNAs) by anodic oxidation as a controllable and cost-effective method in HF aqueous electrolyte in 2001 [13], a large number of researches have been published to improve the geometry of titania nanotubular structures for hydrogen sensing, photoelectrolysis, photocatalysis and dye-sensitized solar cells [8,14,15].

But, TiO_2 films can absorb only a very small UV portion (approximately 4%) of whole solar energy spectrum arriving at the earth's surface. For obtaining a more efficient light harvesting of TiO_2 nanotube, efforts such as doping with other elements (like Ta [16], Ni [17] and N [18,19]) and surface modification with narrow band gap semiconductors (e.g. CdS [20,21], Fe_2O_3 [22], PbS [23], ZnS [24], Ag_2S [25]) have been performed leading to successful increase in their photoresponse under visible light.

* Corresponding author at: Department of Physics, Sharif University of Technology, P.O. Box 11155-9161, Tehran, Iran. Tel.: +98 21 6616 4516; fax: +98 21 6601 2983.
E-mail address: moshfegh@sharif.edu (A.Z. Moshfegh).

http://dx.doi.org/10.1016/j.apcatb.2014.06.053
0926-3373/

Table 1
A brief review of the CdS synthesis methods on the TNA films and the obtained photoresponses.

CdS nanostructure	CdS growth method	Normalized photocurrent (mA/W)	Wavelength (nm)	Electrolyte	Bias voltage (V)[a]	Ref.
Nanoparticle (10–20 nm)	Electrodeposition	~25	>400	1 M Na_2S	0.5	[28]
Thin layer	Electrodeposition	~100	Xe lamp	1 M Na_2S	0.2	[29]
Nanoparticle (~10 nm)	S-CBD	48	Xe lamp	1 M Na_2S	0.2	[30]
Nanoparticle (2–10 nm)	S-CBD	56.5	>400	1 M Na_2S	0.0	[31]
Nanoparticle (~10 nm)	S-CBD	14.3	>300	0.1 M Na_2S	−0.4	[32]
Nanoparticle (~50 nm)	Sonoelectrodeposition	32	>400	1 M Na_2S	0.5	[33]
Quantum dot (~5 nm)	Sonoelectrodeposition	2.0 mA/cm^2[b]	>420	0.5 M Na_2S	0.0	[34]
Quantum dot (~5 nm)	Solvothermal	5.7 mA/cm^2[b]	>420	0.1 M Na_2S	0.0	[35]
Quantum dot (5–10 nm)	S-CBD	14.6	Solar simulator	0.5 M Na_2S; 2 M S; 0.2 M KCl	0.0	[36]
Nanoparticle	Sonication-assisted; S-CBD	41.6	Solar simulator	0.5 M Na_2S; 2 M S; 0.2 M KCl	0.0	[26]
Quantum dot (5.6 nm)	Electrostatic attractive interactions	~12 μA/cm^2[b]	>420	0.1 M Na_2SO_4	0.0	[37]
Nanoparticle (~30–50 nm)	S-CBD	70 ± 2	Xe lamp	0.1 M Na_2S	0.1	This work

[a] Bias voltage was measured vs. Ag/AgCl electrode.
[b] No light intensity (with unit of W/cm^2) was mentioned.

Among the semiconducting surface modifiers, CdS (with $E_g \sim 2.4$ eV) is more attractive because of its low cost and simple preparation process. Recent studies on the PEC properties of the CdS modified TNA are summarized in Table 1. Among the various CdS synthesis methods, S-CBD as a solution-based method due its low cost was attended by other researchers [26,27].

In this work, free-standing TNA films have been prepared by anodic oxidation of a Ti foil in NH_4F organic electrolyte. Subsequently, the TNA films have been modified with various amounts of CdS nanoparticles using sequential-chemical bath deposition (S-CBD). The optical properties, crystalline structure and surface chemical state of the annealed TNA films have been determined using appropriate analytical techniques. In addition, a comprehensive study on electrochemical and photoelectrochemical properties of the CdS modified TNAs has been performed for further understanding the function of CdS for the first time. Moreover, an optimum amount of CdS immersion cycle number was determined leading to maximum photocurrent density. A higher photoresponse of the TNA/CdS is accomplished as compared to other published reports by using simillar S-CBD method (see Table 1 for details). Furthermore, the effect of CdS deposition process cycles on trap state and photovoltage variation of TNA/CdS films has been also investigated.

2. Materials and methods

Vertically oriented TiO_2 nanotube array films have been synthesized by using two-step anodization of titanium sheets (99.5% purity, 0.5 mm thickness) in electrolyte solution contained deionized (DI) water and ethylene glycol with ratio 10:90 with 0.1 M NH_4F and small amount of 1 M H_3PO_4 (for reducing the pH to 5.6) [25]. The anodization was carried out at 60 V for 200 min (80 min for first step and 120 min for second step). During the anodization, samples were sonicated for about 30 s between the steps. Crystalline TNAs were formed by annealing the anodized Ti sheet in air at 500 °C for 80 min with heating rate of about 10 °C min^{-1} [38]. TiO_2 particulate films (PF) have been also prepared by TiO_2 nanoparticle paste4SHARIFSOLAR, PST-20T, with the average size of 30 nm) by doctor blade method. Then, the PFs have been annealed in 500 °C for 80 min for comparision. The average thicknesses of the PFs were about ~50 μm.

CdS nanoparticles were deposited on surface on the synthesized TNAs by S-CBD method using the following procedure: The samples were successively immersed in four different beakers for 20 s each; the first beaker contained 0.1 M $Cd(NO_3)_2$ aqueous solution, another contained 0.1 M Na_2S, and the other two contained distilled water to rinse the samples from the excess of each precursor solution. The immersion cycle was repeated for different cycles (n) to synthesized TNA/CdS-n and PF/CdS-n (n = 10, 20, 30). After each rinsing, the samples washed out with DI water to remove loosely bounded CdS and after several cycles, the color of the film became a strong yellow to orange as also observed by other researchers [26,27].

The morphology of the prepared films and their surface chemical composition were characterized by field emission scanning electron microscopy (FE-SEM, Hitachi-S-4160) and X-ray photoelectron spectroscopy (XPS), using monochromatic AlK_α radiation source (1486.6 eV), respectively. All binding energy values were calibrated by fixing the C(1s) core level to the 284.6 eV. All of the peaks were deconvoluted using SDP software (version 4.1) with 80% Gaussian–20% Lorentzian peak fitting. The accuracy in binding energy measurements was ±0.1 eV. The elemental composition of the nanotube array films is also analyzed by Energy Dispersive X-Ray Spectroscopy (EDS, Philips XL-30 ESEM). Moreover, optical absorption spectra of the samples were investigated by UV–visible diffuse reflectance spectroscopy (DRS) from 200 to 1000 nm wavelength with resolution of 1 nm. X-ray diffraction (XRD) analysis with CuK_α radiation source (λ = 1.5410 Å), was also employed to determine crystallinity and phase formation of the annealed samples.

PEC properties of the synthesized TNA/CdS-n thin film photoanodes such as photocurrent density response (J) and open circuit voltage (V_{oc}) were studied using 0.1 M Na_2S (pH = 13.2) solution as electrolyte. It is well-known that Na_2S electrolyte solution is an efficient hole scavenger for CdS in which the electrodes are stable [28,39]. All PEC measurements were carried out using three-electrode configuration galvanostat/potentiostat (Autolab PGSTAT302) with a Pt counter electrode and Ag/AgCl reference electrode. The working electrode (TNA/CdS-n thin film photoanodes) was illuminated with solar like light source (Xenon short arc lamp (OSRAM 5000 W HBM/OFR)) during a voltage sweep from −0.6 to 1.0 V (versus Ag/AgCl) with a constant sweep rate of 1 mV/s. To perform the measurements at room temperature, a glassy IR filter has been placed in front of the lamp. The photocurrent dynamics of the electrode was recorded according to changes in response to sudden switching on and off at constant input power of 400 mW/cm^2 at a bias voltage of 0.1 V (vs. Ag/AgCl). The incident photon to current efficiency (IPCE) of the samples was also investigated as a function of incident wavelength (λ) at constant illumination intensity.

3. Results and discussion

3.1. The characterization of TNA/CdS-n films

The FE-SEM top view image of the pure TNAs after annealing in air at 500 °C for 80 min presented in Fig. 1(a). According to image analysis, the average inner diameter and the wall thickness of the annealed samples were 125 ± 6 and 38 ± 3 nm, respectively. The inset in Fig. 1(a) also depicted the cross sectional view of the pure annealed TNAs showing highly ordered and oriented morphology with about 2.9 ± 0.3 μm in length. Fig. 1(b)–(d) shows the FE-SEM images of the TNA/CdS-*n* with *n* = 10, 20 and 30. While the wall thickness of the TNA/CdS-*n* was similar to that of the pure TNA, little CdS nanoparticle (~30–50 nm) clusters were observed on the regularly arranged tube mouth as also seen by others [40]. The TNA/CdS-*n* films showed high orientation and open top characteristics for $n \leq 20$ without losing their structures after CdS nanoparticle deposition. But, it can be seemed the mouth of some nanotubes was closed with increasing the number of immersion cycle. It should be noted that the opening of nanotube mouth and the optimum amount of CdS nanoparticles are essential for a high PEC activity as also reported by others [22,41].

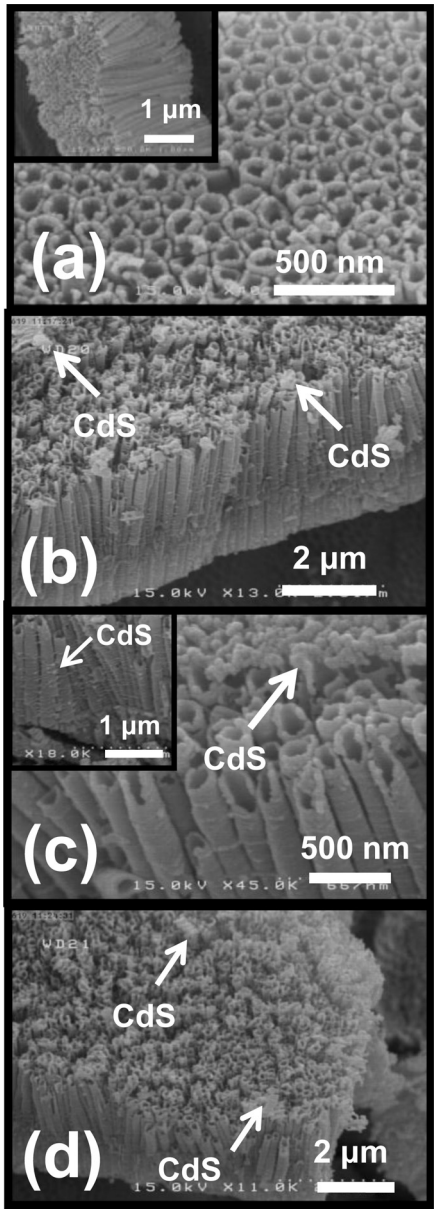

Fig. 1. FE-SEM images of various TNAs/CdS-*n* systems: (a) pure TNA, (b) TNA/CdS-10, (c) TNA/CdS-20 and (d) TNA/CdS-30. *Inset*: Cross-sectional view of the pure TNA. Arrows show the presence of CdS nanoparticles.

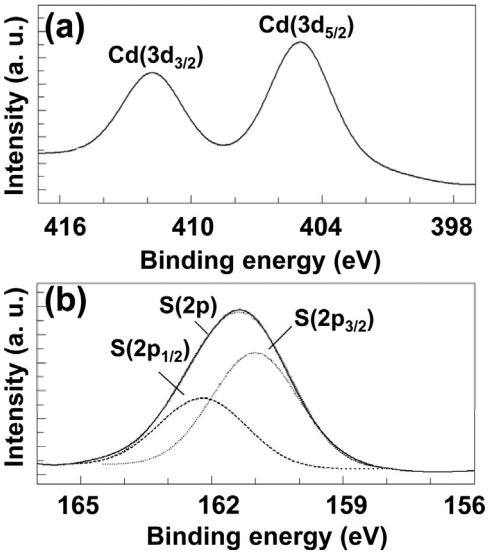

Fig. 2. (a) Cd(3d) and (b) S(2p) core level XPS window spectra of the TNA/CdS-20 film.

In order to determine surface chemical composition and oxidation state of CdS on the annealed TNA samples, XPS measurements were performed. XPS survey spectrum analysis of the TNA/CdS-20 (not shown here) indicated that only Ti, O, Cd, S and a trace amount of carbon exist on the film surface. The carbon was stemmed from the air pollution and or CO/CO_2 adsorption on the surface of the samples.

Fig. 2(a) shows the high resolution XPS spectra of the core level Cd(3d) peak which contains $Cd(3d_{5/2})$ and $Cd(3d_{3/2})$ peaks due to spin-orbit splitting located at binding energy of 404.8 and 411.5 eV, respectively [42,43]. This means that the cadmium is in its elemental chemical state of Cd^{2+}. The spin-orbit splitting components of the core level S(2p) peak was also deconvoluted into two curves: one at 161.0 eV for the $S(2p_{3/2})$ and another at 162.2 eV for the $S(2p_{1/2})$ [42,44] (Fig. 2(b)). These two deconvoluted peaks are corresponding to core level binding energies of the sulfur in CdS composition as also seen and reported before [42]. The difference in binding energy of the corresponding peaks is measured 1.2 eV and the area ratio (2:1) shows an excellent agreement with published values of the S(2p) signal for CdS [32]. Using the area surrounded by each peak, the atomic concentrations of O, Ti, Cd and S were determined 62.7%, 14.6%, 12.1% and 10.6%, respectively. The Cd/S was measured 1.14. These results indicated that the fabricated CdS nanoparticles were slightly Cd rich. This is expected for CdS under normal synthesis conditions as also reported by others (see for example [32,45]). Moreover, EDS spectrum (not shown here) of the TNA/CdS-20 has indicated the presence of the Ti, O, Cd, and S with the weight percent of 61. 1%, 26.7%, 6.5% and 5.7%, respectively, confirming that the CdS is formed in the film.

Fig. 3 illustrates the UV–visible absorption spectra of the TNA/CdS-*n* samples with different CdS deposition process cycles (*n*) as compared to the pure TNAs (*n* = 0). As shown in the figure, the absorption onset of the pure TNAs is located at ~380 nm; which well matched with the band gap energy of TiO_2 in anatase phase [45]. The absorption in visible region enhanced significantly with increasing CdS content. This optical modification in TNA/CdS-*n* systems favors the absorption in visible region of the solar spectrum which is useful in photoelectrochemical applications.

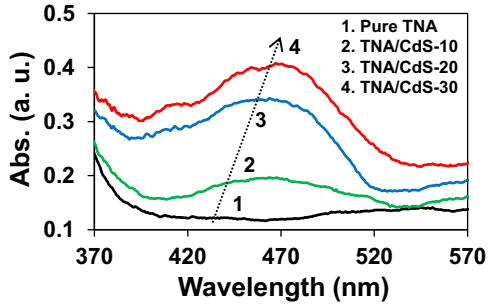

Fig. 3. UV–visible absorption spectra of the TNA/CdS-n (n = 10, 20 and 30 cycles) as compared to pure TNA (n = 0).

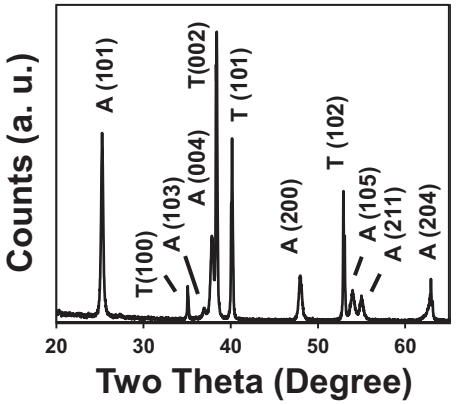

Fig. 4. XRD spectrum of the CdS/TNA-20 film. T and A stand for Ti sheet and anatase crystal phase of TNAs, respectively.

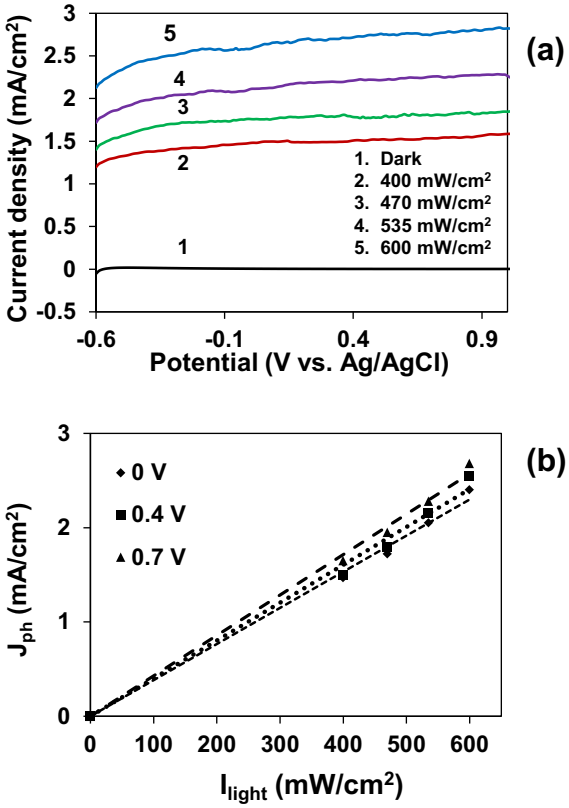

Fig. 5. The photocurrent density of the pure TNA, versus (a) applied potential and (b) illuminating light intensity at three different bias voltages.

Fig. 4 illustrates XRD results of CdS modified TNA sample (n = 20). A similar diffraction spectrum was also obtained for other cycles (and also for pure TNA). Presence of CdS in the sample did not change the peak position of crystalline TiO_2. The TiO_2 nanotubes were in the anatase crystal phase named (A), which was characterized from the diffraction peak (1 0 1) at $2\theta = 25.3^\circ$. The observed sharp peak was due to the annealing treatment of the TNAs before deposition of CdS. In spite of CdS detection by XPS and EDS, no peak was detected for crystalline CdS nanoparticles because of our CdS included films have been not annealed. Another peak (T) was attributed to Ti sheet used as substrate. By applying the Scherrer's equation described as $D = (0.9\lambda)/(\beta \cos\theta)$, where λ is the wavelength of the incident X-ray radiation, β is the full-width at half-maximum (FWHM) of the desired peak in radians and θ is the Bragg angle [46]. For the main peak A(1 0 1), the average size of TiO_2 nanocrystals was estimated about 30 ± 2 nm.

3.2. PEC measurements

3.2.1. Photoresponse of the samples

To investigate the photosensitivity of the prepared samples, the photocurrent density has been measured in both dark and illuminating conditions, as a function of the applied potential (from −0.6 to 1.0 V). All of the potentials have been recorded versus the Ag/AgCl reference electrode. Fig. 5(a) shows the measured photocurrent density for the pure TNA as a function of applied potential, at different illumination intensities. It is clear that the current density under dark is negligible. According to our data analysis, the photoresponse of the pure TNA sample in the whole measured potential ranges was anodic and increased with increasing the light intensity as also reported by other researches (see for example [47]).

To illustrate the relationship between the generated photocurrent density (J_{ph}) and the applied illumination intensity (I_{light}), various J_{ph} as a function of I_{light} were plotted at three selected potentials in a range from zero to 0.7 V (Fig. 5(b)). Logically, a linear relation between J_{ph} and I_{light} has been obtained in all potentials suggesting that charge carriers (e^-–h^+ pair) generation is the rate limiting step [48]. Extrapolations of least-square fitted lines did not pass from the origin and crossed the abscissa in the slight positive values. These values are almost same and equal to the measured dark current (Fig. 5(a)) for each applied potential.

3.2.2. Effect of CdS loading

The photoresponse of the pure PF, PF/CdS-20, pure TNA and CdS modified TNA was compared by using chronoamperometery technique and measuring the photocurrent density (J) at a fixed applied bias potential (+0.1 V vs. Ag/AgCl reference electrode). As shown in Fig. 6, upon illumination of the photoanode surface, rapid generation of photocurrents has been measured for both pure and CdS modified samples. The photocurrent response varied with CdS immersion cycle number, and the maximum photocurrent density (at steady state) of 28 ± 1 mA/cm^2 (or 70 ± 2 mA/W) was obtained for the TNA/CdS-20 photoanode, which is about 30 times higher than the one achieved for the pure TNA. This result is more than all nanoparticular CdS modified TNA reported up to now (see Table 1). Further increasing deposition process cycles from 20 to 30, the photocurrent density of the TNA/CdS-30 sample was decreased due to slowing down the electron injection process [22,41] and blockage of nanotubes's mouths [32]. We are suggesting when the nanotubes are covered with excess CdS, the effective surface area participating in reduction/oxidation processes is reduced and the probability of the photo-generated e^--h^+ recombination is increased resulting in lower J_{ph} value. This argument was verified by investigation of the observed decay in the J_{ph}–t curves. Based on literature [47,48] by

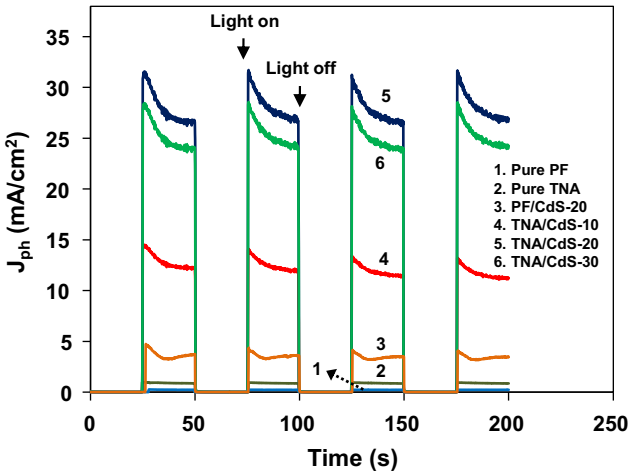

Fig. 6. Photocurrent density response of pure PF, PF/CdS-20, pure TNA and TNA/CdS-*n* (*n* = 10, 20 and 30) in Na_2S solution at 0.1 V bias.

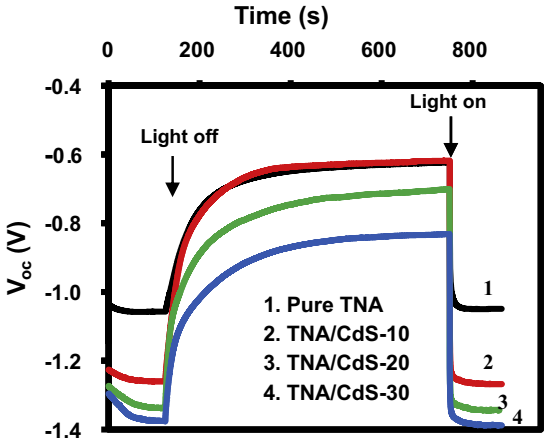

Fig. 7. Open-circuit photovoltage in light on–off process for the pure TNA and TNA/CdS-*n* films.

studying the rate of this decay a time constant called e^--h^+ transport life time can be obtained for each system. This quantity was measured 12.1, 5.6, 3.4 and 2.8 s for the samples with *n* = 0, 10, 20 and 30, respectively. This result was attributed to reduction of TNA surface for higher CdS loading which is in agreement with the proposed mechanism (which will be also discussed later).

Besides, all the modified samples exhibited a better performance than the pure TiO_2 because of visible activity of CdS. A similar behavior has been also seen for the TNA/Fe_2O_3 [22] and CdS/CdSe [41] systems. It should be noted that the observed patterns of photocurrent density response were extremely reproducible for more than 50 light on-off cycles of illuminations and they show only <5% reduction.

To understand the role of TiO_2 nanotube arrays, we have prepared PF and PF/CdS-20 samples. Moreover, a comparison between the pure PF and pure TNA was examined. We have found that the one-dimensional (1D) nanostructures of TiO_2 are more efficient than TiO_2 particulate film (Fig. 6). This result agrees with other published report indicating that the TNAs provide unique electronic properties, such as high electron mobility or quantum confinement effects and a very high specific surface area [14]. Hence, it has brought about that TNA/CdS-20 obtained a higher photocurrent density than the PF/CdS-20. Based on our data analysis, the photocurrent density of CdS modified TNA was about 7 times higher than CdS modified PF.

Regarding the utilized electrolyte was water based (0.1 M aqueous solution of Na_2S), it is worthy to note that the recorded currents were related to primarily the photogenerated hole captured by Na_2S and partially oxidation of H_2O to O_2 on the electrode/electrolyte interface. Hence, this phenomenon can be considered as water splitting reaction (in presence of Na_2S solution) which is potentially applicable for clean solar hydrogen production.

Open-circuit photovoltage (V_{oc}) decay measurements were also employed to investigate the charge collection properties of the TNA/CdS-*n*. In this case, the samples were exposed to Xe lamp with a constant power of 400 mW/cm^2 for 125 s before turning off the light. Transient values of the open circuit potential were measured as a function of time for 625 s after the illumination was turned off. As shown in Fig. 7, the photopotential of CdS modified TNAs reduced with increasing the deposition process cycles indicating that the free electron density in the photoanode nanostructure increased with *n*, under similar illumination condition [49]. So, there are more photoelectrons accumulated on the surface of the TNA/CdS-*n* as compared to the pure TNA. The V_{oc} value of the samples was increased from −1.06 V for the pure TNA to −1.33 V for the TNA/CdS-20 sample. Upon stopping the illumination, the potential decays slowly as the stored electrons leak out of the nanotube arrays. The slow decay rate indicates a long lifetime of the e^--h^+ pair in presence of CdS nanoparticles, exhibiting a high photo activity [22]. This phenomenon can be also followed by measuring electron life time (τ_n) from the curves using the following equation [50]:

$$\tau_n = -\frac{k_B T}{e}\left(\frac{dV_{oc}}{dt}\right)^{-1} \quad (1)$$

where k_B, T and e are the Boltzman constant, temperature in Kelvin and electron charge, respectively. We have calculated this quantity and the result shows that τ_n was about 23, 27 and 30 ms for *n* = 0, 10 and 20, respectively. For the sample with 30 immersion cycles of CdS loading, the life time was almost similar to *n* = 20. Thus, loading of CdS up to *n* = 20 increase photogenerated carrier life time.

To investigate the change in photo-response of the TNA/CdS-*n* films as a function of the irradiation wavelengths (λ), IPCE of the samples has been measured using the following relation [1]:

$$\text{IPCE\%} = \frac{c \times h}{e}\frac{J_{ph}\,(\text{A cm}^{-2})}{\lambda\,(\text{nm}) \times P\,(\text{W cm}^{-2})} \times 100 \quad (2)$$

here J_{ph} (A cm^{-2}) and P (W cm^{-2}) are photocurrent density and the intensity of illuminating light at each wavelength, respectively. The obtained results are demonstrated in Fig. 8(a). It can be seen that for the all synthesized photoanodes, the best PEC performance, occurred in the wavelength range of 380–400 nm which agrees with the absorption edge of the TiO_2. Moreover, the observed enhancement in UV region was due to the e^--h^+ recombination delay time made by addition of CdS nanoparticles as measured from V_{oc} study (see Fig. 7). As shown in Fig. 8(a), the IPCE value in the visible region increased with increasing the immersion cycle number. Furthermore, the IPCE value in the visible region of the samples reached to maximum value of ~20% at wavelength of 430 nm for the TNA/CdS-20. Considering the fact that visible active semiconductor in the synthesized photoanodes is CdS, the observed enhancement for this sample is due to activity of CdS in visible region of solar spectrum.

To elucidate the mechanism of photoenhancement, we have proposed a simple model based on the amount of CdS concentrations (low and high concentrations). The IPCE was decreased for higher immersion cycle (i.e. *n* = 30) due to two mechanisms, as have been represented in Fig. 8(b): (1) an electron has more chance to be trapped (I) or recombined (II) with holes in the CdS valence band and (2) CdS nanoparticles cause pore blockage (III) as shown in the SEM images. Therefore, electrons could not successfully

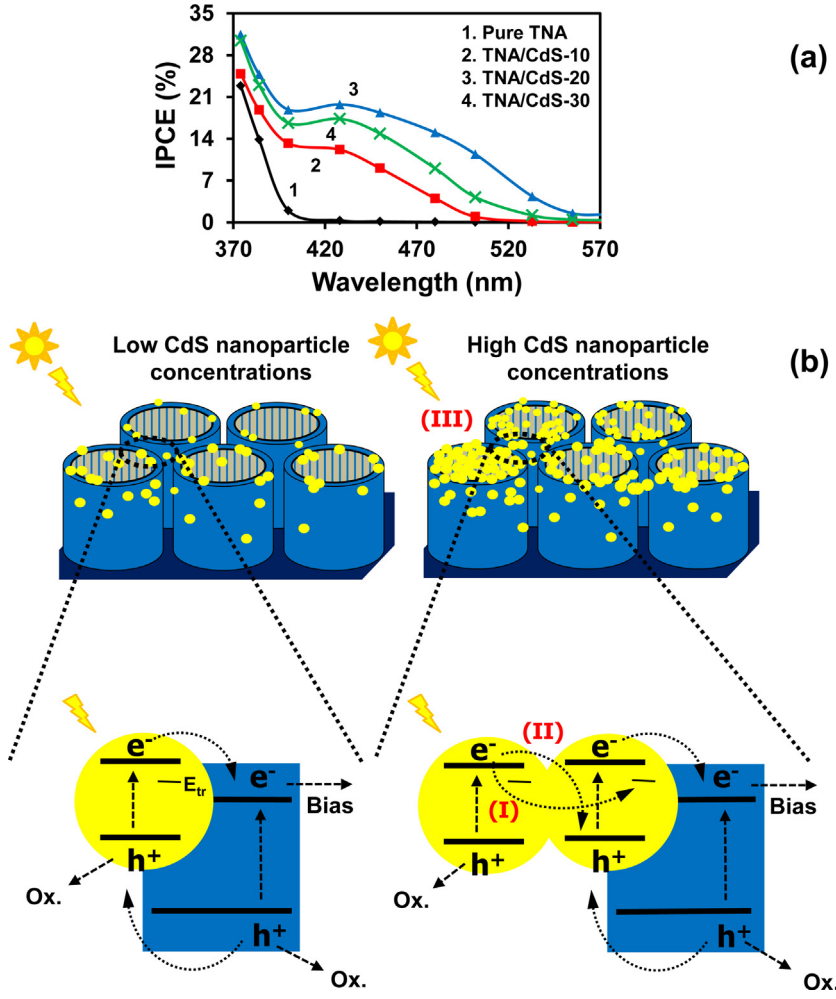

Fig. 8. (a) Incident photon-to-current efficiency (IPCE) or "action spectra" of the samples versus irradiated wavelength under constant illumination intensity. (b) The proposed mechanism for CdS dual function in nanotubular TiO_2 photoanode. E_{tr} represents energy of trap states.

penetrate into the deeper part of the TNAs, and the holes could not be scavenged by electrolyte at surface for high concentrations [41]. This IPCE's measurements are in complete agreement with the result obtained from our chronoamperometery analysis.

3.2.3. Trap states study

From the electrochemical impedance spectroscopy (EIS), one can find the total capacitance C at the solid/electrolyte interface and draw the so called Mott–Schottky plot (C^{-2} as a function of the applied voltage V_a). The quantity of C depends on the flat band (V_{fb}) potential described by the following relation [51]:

$$\frac{1}{C^2} = \frac{2}{\varepsilon\varepsilon_0 N_D e A^2}\left(V_a - V_b - \frac{K_B T}{e}\right) \quad (3)$$

where e is the electron charge, N_D represents the donor density, ε is the dielectric constant of the semiconductor (in here TiO_2), ε_0 is the vacuum permittivity, T is the absolute temperature, k_B is the Boltzman constant and A is the surface area of the electrode. Using this relation and the related Mott-Shottky plots for the samples (not shown here), the value for the flat band potential has been measured about 1.0 ± 0.1 V for the all pure and CdS loaded samples which is in agreement with the V_{fb} value reported before for TiO_2 photoanode [48,52]. Moreover, the donor density was obtained at about $(37 \pm 2) \times 10^{19}$ cm^{-3} for the pure TNA and all the TNA/CdS-n samples. Hence, it can be concluded that loading CdS on TNA films has caused no significant change in N_D value.

To investigate the trap states of the samples, we have utilized the method described in [53]. First, the TNA/CdS-n polarized at 0 V for a few minutes. Then, the potential was shifted immediately to a value more positive than V_{fb} ($V > -1.0$ V in here) and the current was registered for a certain time. As soon as negative potential was applied, a sharp cathodic peak was observed. Then, the current decayed very quickly. The accumulated charge density (Q/A) in the layer was calculated by integrating the measured current–time curves. The obtained results can be understood in terms of trap filling in the band gap region. For the all samples, when the applied potential shifted negatively, the accumulated charges in the films increased significantly indicating that more trap states are present in the potentials close to flat band level [52].

It is well known that accumulated charge reflects density of trap states by the following relation [53]:

$$N_{trap}(V) = \frac{(dQ/A)}{e\,dV} \quad (4)$$

here, V is applied potential, e is the elementary charge, $N_{trap}(V)$ is the density of traps as a function of applied potential and Q/A is the surface charge density. Therefore, by calculating the derivative of the Q–V plots (Fig. 9); a direct measure of trap distribution can be obtained [51]. As expected, the measured trap density ($N_{trap}(V)$) increased in the potentials near to flat band level. This behavior was nearly same for the all synthesized TNA/CdS-n samples. A similar

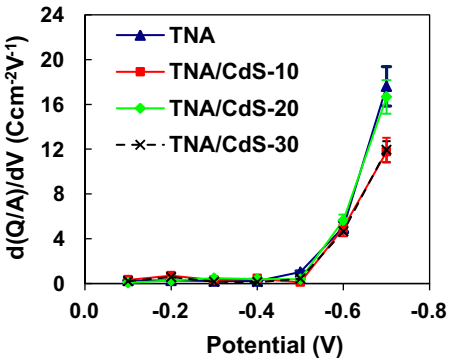

Fig. 9. d*Q*/Ad*V* distribution versus applied bias potential for the TNA/CdS-*n*.

behavior also observed for the Ag:TiO_2 nanocomposite photoanodes very recently for different Ag concentrations [52].

4. Conclusions

In summary, the TiO_2 nanotube array photoelectrode films were fabricated using anodization technique. The produced nanotube array films exhibit highly ordered nanostructure based on our FE-SEM observations. Anatase phase formation of the TNA with an average crystalline size of 30 ± 2 nm has been detected. The CdS nanoparticles were deposited on the pure TNA by S-CBD method with different immersion cycles. X-ray photoelectron spectroscopy determined CdS nanoparticles (slightly Cd rich) successfully loaded on the surface of the pure TNA. The UV–visible absorption spectra of the samples showed the absorption of CdS modified TNAs increased in visible region. By optimizing the CdS deposition cycles, the highest photocurrent density of 28 ± 1 mA/cm^2 was achieved under solar like light source illumination. The obtained photocurrent density (or 70 ± 2 mA/W) was not only greater than other published results, but also has been achieved by applying a very low bias voltage 0.1 V. This obtained photocurrent density in the PEC cell, can be efficiently used in hydrogen generation and other solar energy applications.

References

[1] B. AlOtaibi, H.P.T. Nguyen, S. Zhao, M.G. Kibria, S. Fan, Z. Mi, Nano Lett. 13 (2013) 4356–4361.
[2] A. Paracchino, V. Laporte, K. Sivula, M. GrÃ¤tzel, E. Thimsen, Nat. Mater. 10 (2011) 456–461.
[3] M. Altomare, M. Pozzi, M. Allieta, L.G. Bettini, E. Selli, Appl. Catal. B-Environ. 136 (2013) 81–88.
[4] A. Fujishima, K. Honda, Nat. Mater. 238 (1972) 37–38.
[5] A.Z. Moshfegh, J. Phys. D: Appl. Phys. 42 (2009) 233001.
[6] J. Miao, H.B. Yang, S.Y. Khoo, B. Liu, Nanoscale 5 (2013) 11118–11124.
[7] R. Sanchez-Tovar, K. Lee, J. Garcia-Anton, P. Schmuki, ECS Electrochem. Lett. 2 (2013) H9–H11.
[8] I. Paramasivam, H. Jha, N. Liu, P. Schmuki, Small 8 (2012) 3073–3103.
[9] I.S. Cho, Z. Chen, A.J. Forman, D.R. Kim, P.M. Rao, T.F. Jaramillo, X. Zheng, Nano Lett. 11 (2011) 4978–4984.
[10] M. Pelaez, N.T. Nolan, S.C. Pillai, M.K. Seery, P. Falaras, A.G. Kontos, P.S.M. Dunlop, J.W.J. Hamilton, J.A. Byrne, K. O'Shea, M.H. Entezari, D.D. Dionysiou, Appl. Catal. B-Environ. 125 (2012) 331–349.
[11] X. Chen, S.S. Mao, Chem. Rev. 107 (2007) 2891–2959.
[12] S. Li, J. Qiu, M. Ling, F. Peng, B. Wood, S. Zhang, ACS Appl. Mater. Interfaces 5 (2013) 11129–11135.
[13] D. Gong, C.A. Grimes, O.K. Varghese, W.C. Hu, R.S. Singh, Z. Chen, E.C. Dickey, J. Mater. Res. 16 (2001) 3331–3334.
[14] P. Roy, S. Berger, P. Schmuki, Ang. Chem. Int. Ed. 50 (2011) 2904–2939.
[15] S. Rani, S.C. Roy, M. Paulose, O.K. Varghese, G.K. Mor, S. Kim, S. Yoriya, T.J. LaTempa, C.A. Grimes, Phys. Chem. Chem. Phys. 12 (2010) 2780–2800.
[16] M. Altomare, K. Lee, M.S. Killian, E. Selli, P. Schmuki, Chem.–Eur. J. 19 (2013) 5841–5844.
[17] J. Chattopadhyay, R. Srivastava, P.K. Srivastava, J. Appl. Electrochem. 43 (2013) 279–287.
[18] H.J. Yun, D.M. Lee, S. Yu, J. Yoon, H.-J. Park, J. Yi, J. Mol. Catal. A: Chem. 378 (2013) 221–226.
[19] H. Fakhouri, J. Pulpytel, W. Smith, A. Zolfaghari, H.R. Mortaheb, F. Meshkini, R. Jafari, E. Sutter, F. Arefi-Khonsari, Appl. Catal. B-Environ. 144 (2014) 12–21.
[20] F.L. Su, J.W. Lu, Y. Tian, X.B. Ma, J.L. Gong, Phys. Chem. Chem. Phys. 15 (2013) 12026–12032.
[21] G. Zhu, L. Pan, T. Xu, Z. Sun, ACS Appl. Mater. Interfaces 3 (2011) 1472–1478.
[22] S.Y. Kuang, L.X. Yang, S.L. Luo, Q.Y. Cai, Appl. Surf. Sci. 255 (2009) 7385–7388.
[23] Q. Kang, S. Liu, L. Yang, Q. Cai, C.A. Grimes, ACS Appl. Mater. Interfaces 3 (2011) 746–749.
[24] Q. Shen, J. Kobayashi, L.J. Diguna, T. Toyoda, J. Appl. Phys. 103 (2008) 084304.
[25] M. Gholami, M. Qorbani, O. Moradlou, N. Naseri, A.Z. Moshfegh, RSC Adv. (2013) 7838–7844.
[26] X. Ma, Y. Shen, G. Wu, Q. Wu, B. Pei, M. Cao, F. Gu, J. Alloys Compd. 538 (2012) 61–65.
[27] G. Limin, W. Xiaohui, Z. Caifu, L. Longtu, J. Phys. D: Appl. Phys. 44 (2011) 165403.
[28] S. Chen, M. Paulose, C. Ruan, G.K. Mor, O.K. Varghese, D. Kouzoudis, C.A. Grimes, J. Photochem. Photobiol. A: Chem. 177 (2006) 177–184.
[29] Y. Yuxin, J. Zhengguo, H. Feng, Nanotechnology 18 (2007) 495608.
[30] J. Bai, J.H. Li, Y.B. Liu, B.X. Zhou, W.M. Cai, Appl. Catal. B-Environ. 95 (2010) 408–413.
[31] W.-T. Sun, Y. Yu, H.-Y. Pan, X.-F. Gao, Q. Chen, L.-M. Peng, J. Am. Chem. Soc. 130 (2008) 1124–1125.
[32] C.J. Lin, Y.H. Yu, Y.H. Liou, Appl. Catal. B: Environ. 93 (2009) 119–125.
[33] Y. Liu, H. Zhou, B. Zhou, J. Li, H. Chen, J. Wang, J. Bai, W. Shangguan, W. Cai, Int. J. Hydrogen Energy 36 (2011) 167–174.
[34] Y. Xie, G. Ali, S.H. Yoo, S.O. Cho, ACS Appl. Mater. Interfaces 2 (2010) 2910–2914.
[35] S.S. Kalanur, S.H. Lee, Y.J. Hwang, O.-S. Joo, J. Photochem. Photobiol. A: Chem. 259 (2013) 1–9.
[36] D. Li, N. Pan, J. Liao, X. Cao, S. Lin, Int. J. Photoenergy 2013 (2013) 10.
[37] F.-X. Xiao, J. Miao, H.-Y. Wang, B. Liu, J. Mater. Chem. A 1 (2013) 12229–12238.
[38] J.M. Macák, H. Tsuchiya, P. Schmuki, Angew. Chem. Int. Ed. 44 (2005) 2100–2102.
[39] K. Nagasuna, T. Akita, M. Fujishima, H. Tada, Langmuir 27 (2011) 7294–7300.
[40] H. Cheng, X. Zhao, X. Sui, Y. Xiong, J. Zhao, J. Nanopart. Res. 13 (2011) 555–562.
[41] H. Shuqing, Z. Quanxin, H. Xiaoming, G. Xiaozhi, D. Minghui, L. Dongmei, L. Yanhong, S. Qing, T. Taro, M. Qingbo, Nanotechnology 21 (2010) 375201.
[42] S. Chandramohan, R. Sathyamoorthy, P. Sudhagar, D. Kanjilal, D. Kabiraj, K. Asokan, V. Ganesan, T. Shripathi, U.P. Deshpande, Appl. Phys. a-Mater. Sci. Process. 94 (2009) 703–714.
[43] R. Poulomi, S. Suneel Kumar, J. Phys. D: Appl. Phys. 39 (2006) 4771.
[44] D.A. Mazón-Montijo, M. Sotelo-Lerma, M. Quevedo-López, M. El-Bouanani, H.N. Alshareef, F.J. Espinoza-Beltrán, R. Ramírez-Bon, Appl. Surf. Sci. 254 (2007) 499–505.
[45] C.A. Grimes, G.K. Mor, TiO_2 Nanotube Arrays: Synthesis, Properties, and Applications, Springer, 2009.
[46] B.D. Cullity, Elements of X-Ray Diffraction, Addison-Wesley, 1978.
[47] N. Naseri, P. Sangpour, A.Z. Moshfegh, Electrochim. Acta 56 (2011) 1150–1158.
[48] N. Naseri, M. Yousefi, A.Z. Moshfegh, Solar Energy 85 (2011) 1972–1978.
[49] M.A. Butler, J. Appl. Phys. 48 (1977) 1914–1920.
[50] A. Zaban, M. Greenshtein, J. Bisquert, ChemPhysChem 4 (2003) 859–864.
[51] A.J. Bard, L.R. Faulkner, Electrochemical Methods: Fundamentals and Applications, Wiley, 2000.
[52] N. Naseri, H. Kim, W. Choi, A.Z. Moshfegh, Int. J. Hydrogen Energy 37 (2012) 3056–3065.
[53] H.L. Wang, J.J. He, G. Boschloo, H. Lindstrom, A. Hagfeldt, S.E. Lindquist, J. Phys. Chem. B 105 (2001) 2529–2533.